Supplementary Information

for

Effects of Geometrical Isomerism on Emissive Behaviour of Heteroleptic Cyclometalated Ir(III) Complexes

Yoshiki Jinsenji,[a] Kazuyoshi Takimoto,[a] Jun Yoshida,[b] Shigeki Mori,[c] Yutaka Watanabe,[a] and Hisako Sato*[a]

[a] Graduate School of Science and Engineering, Ehime University, Matsuyama 790-8577, Japan

[b] Department of Chemistry, Kitasato University, Sagamihara 252-0329, Japan

[c] Advanced Research Support Center, Ehime University, Matsuyama 790-8577, Japan

Contents:

S1. Chromatographic separation of *cis*-(N,N) and *trans*-(N,N) isomers of [Ir(bzq)$_2$(PBO)]

The chromatogram for separating *cis*-(N,N) and *trans*-(N,N) isomers of [Ir(bzq)$_2$(PBO)] on a HPLC silica gel column is shown below.

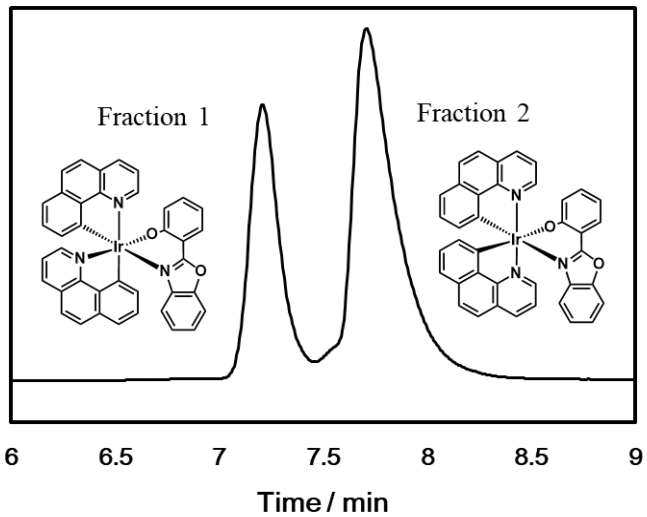

Figure S1. The chromatogram of [Ir(bzq)$_2$(PBO)] when it was upon the subjection to HPLC silica gel column. Fractions 1 and 2 correspond to *cis*-(N,N) and *trans*-(N,N) isomers, respectively, as described in the text. An eluting solvent was 10:1 (v/v) CH_2Cl_2 (MeOH 0.01%) and hexane. A flow rate was 2.5 mL min^{-1} and the monitoring wavelength was 525 nm.

S2. ^{1}H NMR, ^{13}C NMR, MS data and elemental analysis

[Ir(bzq)$_2$Cl]$_2$: δH (400 MHz; $CDCl_3$) 5.98 (2H, d, *J*=7.3 Hz), 6.81 (2H, t, *J*=7.6 Hz), 7.17 (2H, dd, *J*=8.0 and 5.5 Hz), 7.21 (2H, d, *J*=8.0 Hz), 7.69 (2H, d, *J*=8.8 Hz), 7.76 (2H, d, *J*=8.8 Hz), 8.28 (2H, d, *J*=7.1 Hz), 9.36 (2H, d, *J*=4.4 Hz)

***cis*-(N,N)-[Ir(bzq)$_2$(PBO)]:** δH (400 MHz; $CDCl_3$) 5.46 (1H, d, *J*=8.0 Hz), 6.48 (1H, dd, *J*=7.0 and 1.0 Hz), 6.51 (1H, ddd, *J*=8.0 and 6.8 and 1.0 Hz), 6.63 (1H, td, *J*=8.0 and 1.0 Hz), 6.68 (1H, dd, *J*=8.8 and 1.0 Hz), 6.89 (1H, dd, *J*=8.0 and 5.5 Hz), 6.99 (1H, t, *J*=8.0 Hz), 7.03 (1H, td, *J*= 8.0 and 1.0 Hz), 7.11 (1H, ddd, *J*=8.8, 6.8 and 1.8 Hz), 7.30 (1H, d, *J*=8.0 Hz), 7.41 (1H, d, *J*=8.0 Hz), 7.44 (1H, dd, *J*=8.0 and 5.0 Hz), 7.48 (1H, d, *J*=8.8 Hz), 7.54 (1H, t, *J*=8.0 Hz), 7.58 (1H, td, *J*=7.8 and 1.0 Hz), 7.64 (1H, d, *J*=8.8 Hz), 7.78 (1H, dd, *J*=5.5 and 1.0 Hz), 7.80 (1H, d, *J*=8.8 Hz), 7.83 (1H, d, *J*=8.8 Hz), 7.86 (1H, dd, *J*=8.0 and 1.0 Hz), 7.93 (1H, dd, *J*=7.8 and 1.0 Hz), 7.95 (1H, dd, *J*=8.0 and 1.8 Hz), 8.24 (1H, dd, *J*=8.0 and 1.0 Hz), 8.56 (1H, dd, *J*=5.0 and 1.0 Hz); δC (125 MHz; CD_2Cl_2) 110.2, 110.9, 114.8, 118.9, 120.1, 120.4, 120.9, 121.2, 121.8, 123.4, 123.7, 123.8, 124.5, 124.6, 124.8, 126.7, 127.0, 127.7, 128.5, 128.8, 129.5, 130.1, 131.3, 133.1, 133.7, 134.4, 134.5, 135.4, 135.5, 136.6, 137.1, 141.9, 147.4, 148.3, 150.7, 153.4, 155.9, 161.1, 169.2; ESI-HRMS, Calcd for $[IrC_{39}H_{24}N_3O_2]^+$ 759.1498, Found 759.1492; Anal. Calcd for $IrC_{39}H_{24}N_3O_2{\bullet}C_6H_{14}$: C, 63.96; H, 4.53; N, 4.97. Found: C, 64.08; H, 4.89; N, 4.47.

***trans*-(N,N)-[Ir(bzq)$_2$(PBO)]:** δH (400 MHz; $CDCl_3$) 5.93 (1H, d, *J*=8.5 Hz), 6.16 (1H, brd, *J*=7.8 Hz), 6.39 (1H, brd, *J*=8.5 Hz), 6.48 (1H, ddd, *J*=8.0 and 6.8 and 1.0 Hz), 6.63 (1H, ddd, *J*=8.5, 7.5 and 1.0 Hz), 6.70 (1H, d, *J*=8.8 Hz), 6.99 (1H, t, *J*=8.0 Hz), 7.00 (1H, t, *J*=7.8 Hz), 7.03 (1H, ddd, *J*=8.5 and 7.5 and 1.0 Hz), 7.19 (1H, ddd, *J*=8.7 and 6.8 and 1.8 Hz), 7.27 (1H, dd, *J*=8.0 and 5.5 Hz), 7.32 (1H, d, *J*=8.0 Hz), 7.34 (1H, d, *J*=7.8 Hz), 7.39 (1H, d, *J*=8.0 Hz), 7.46 (1H, dd, *J*=7.8 and 5.5 Hz), 7.57 (1H, d, *J*=8.8 Hz), 7.61 (1H, d, *J*=8.8 Hz), 7.77 (1H, d, *J*=8.8 Hz), 7.78 (1H, d, *J*=8.8 Hz), 8.00 (1H, dd, *J*=8.0 and 1.8 Hz), 8.13 (1H, dd, *J*=8.0 and 1.0 Hz), 8.16 (1H, dd, *J*=7.8 and 1.0 Hz), 8.45 (1H, dd, *J*=5.5 and 1.0 Hz), 9.16 (1H, dd, *J*=5.5 and 1.0 Hz); δC (125 MHz; $CDCl_3$) 109.8, 110.5, 113.7, 118.4, 118.8, 119.3, 120.8, 120.9, 123.0, 123.2, 124.2, 124.3, 125.5, 126.1, 126.7, 128.7, 128.8, 128.9, 129.4, 129.6, 130.7, 133.5, 133.8, 134.1, 135.7, 141.5, 141.9, 142.5, 144.2, 146.1, 147.6, 147.9, 148.3, 149.2, 158.3, 158.5, 160.1, 165.3, 169.5; ESI-HRMS, Calcd for $[IrC_{39}H_{24}N_3O_2]^+$ 759.1498, Found 759.1492; Anal. Calcd for $IrC_{39}H_{24}N_3O_2{\bullet}H_2O$: C, 60.30; H, 3.37; N, 5.41. Found: C, 60.67; H, 3.32; N, 5.41.

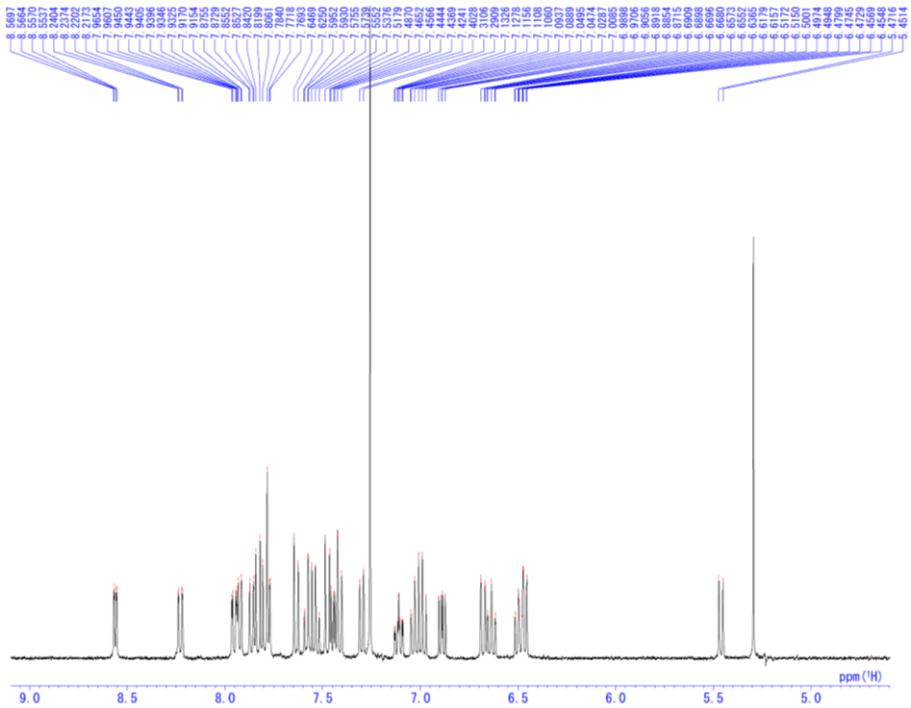

Figure S2. ^{1}H NMR spectrum of *cis*-(N,N)-[Ir(bzq)$_2$(PBO)] (400 MHz; $CDCl_3$).

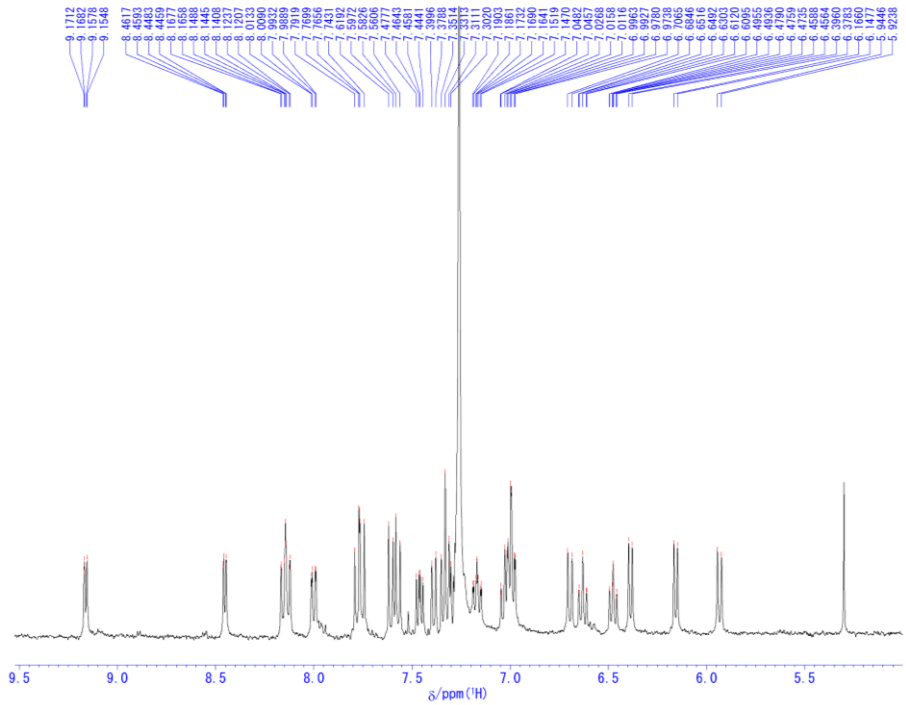

Figure S3. ^{1}H NMR spectrum of *trans*-(N,N)-[Ir(bzq)$_2$(PBO)] (400 MHz; $CDCl_3$).

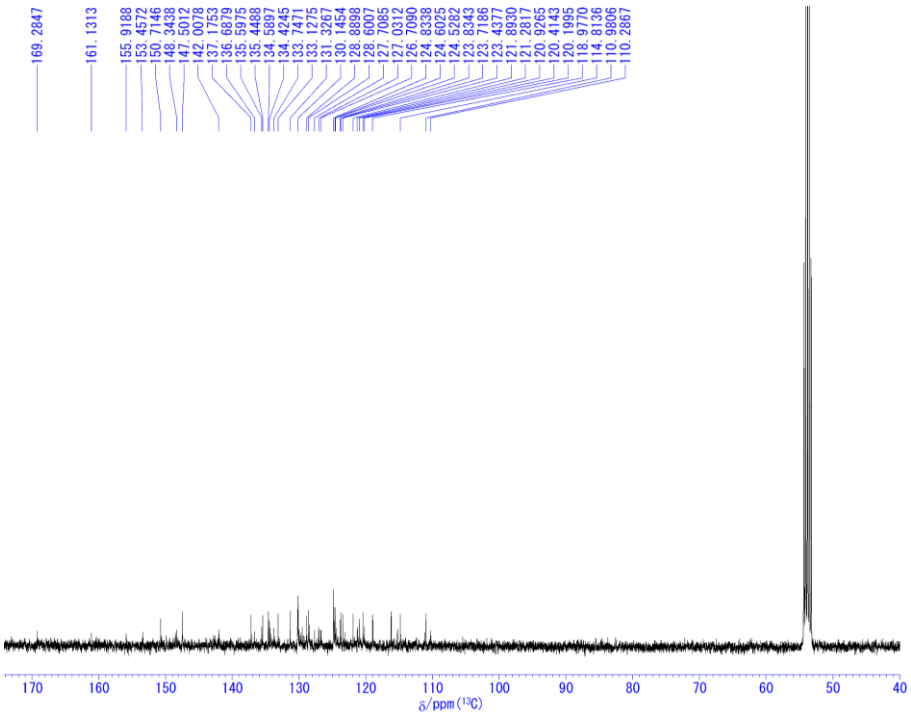

Figure S4. ^{13}C NMR spectrum of *cis*-(N,N)-[Ir(bzq)$_2$(PBO)] (125 MHz; CD_2Cl_2).

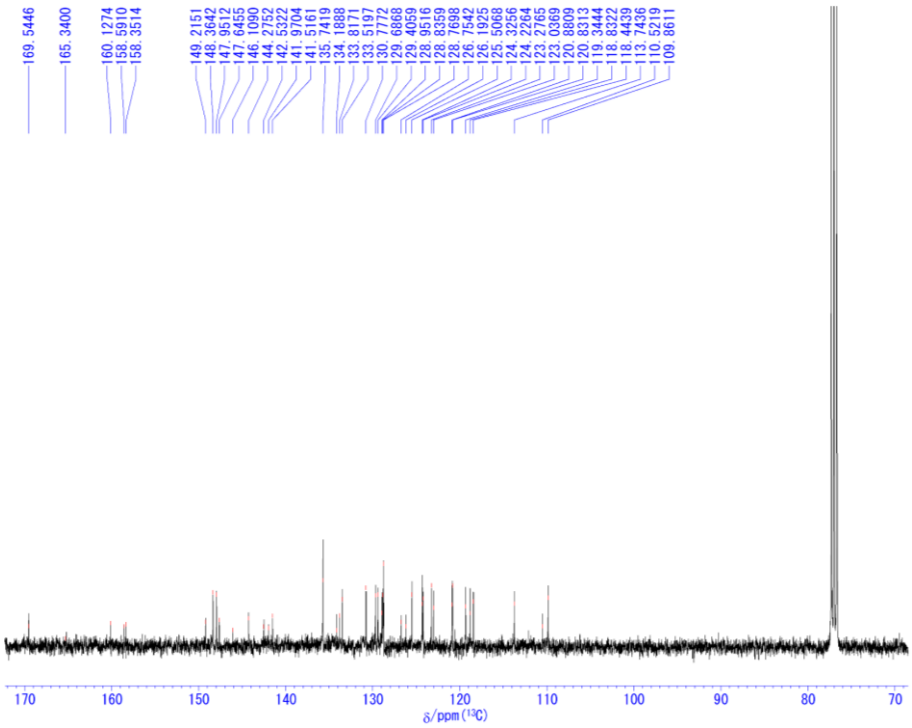

Figure S5. ^{13}C NMR spectrum of *trans*-(N,N)-[Ir(bzq)$_2$(PBO)] (125 MHz; $CDCl_3$).

S3. Optical resolution of [Ir(bzq)$_2$(PBO)] isomers

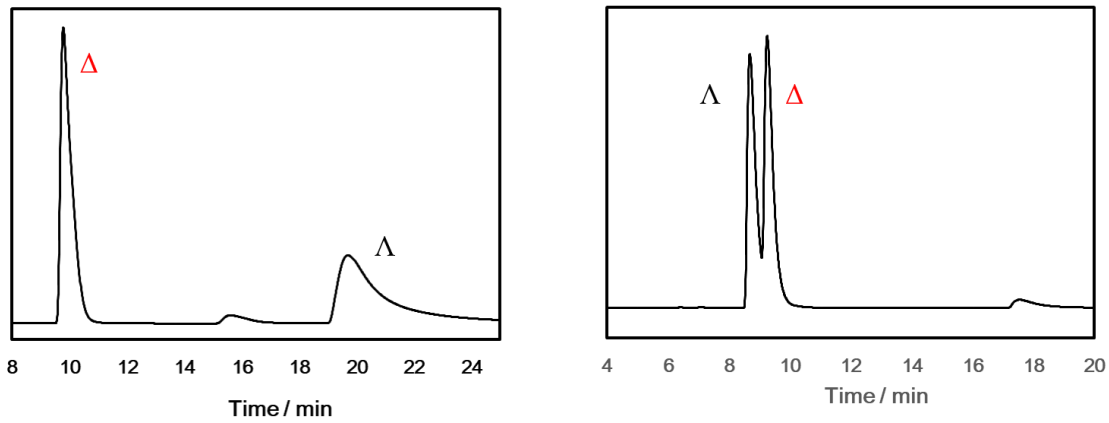

Figure S6. Chromatograms for optical resolution of [Ir(bzq)$_2$(PBO)] isomers: *cis*-(N,N) (left) and *trans*-(N,N) isomers (right). An eluting solvent was CH_2Cl_2. A flow rate was 0.5 mL min^{-1}. The monitoring wavelength was 350 nm. The used column was a CHIRALPACK IC (Daicel, Japan).

S4. Electronic circular dichroism spectra of enantiomeric isomers of [Ir(bzq)$_2$(PBO)]

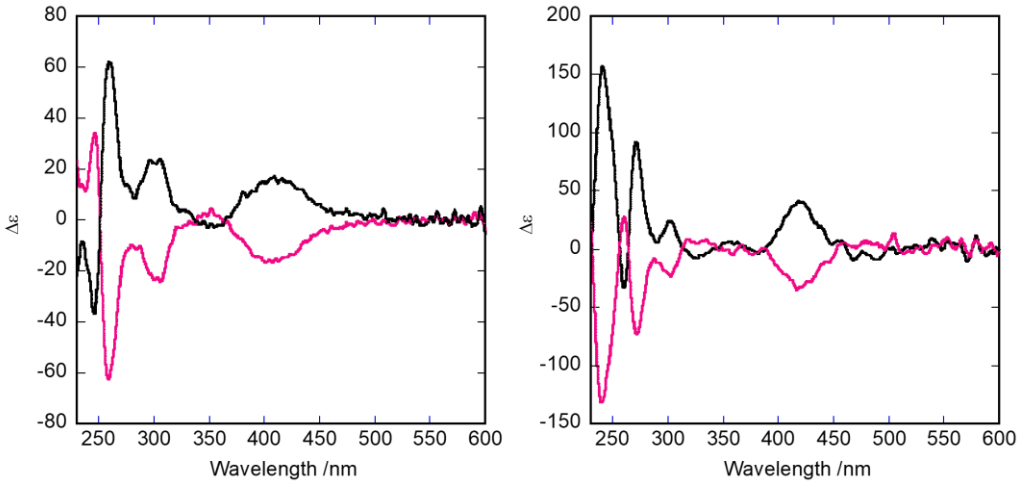

Figure S7. The electronic circular dichroism spectra of *cis*-(N,N) (left) and *trans*-(N,N) isomers (right) of [Ir(bzq)$_2$(PBO)]. The black and red lines correspond to Λ– and Δ–enantiomers, respectively. A solvent was CH_2Cl_2.

S5. Single crystal X-ray analyses of racemic and enantiomeric isomers of [Ir(bzq)$_2$(PBO)]

Single crystal X-ray analyses were performed for both the racemic and enantiomeric forms of [Ir(bzq)$_2$(PBO)] isomers. The preparation of single crystals, crystal data and molecular structures are given below.

Single crystals of Δ-*cis*-(N,N)-[Ir(bzq)$_2$(PBO)] and Λ-*cis*-(N,N)-[Ir(bzq)$_2$(PBO)] were prepared by slow evaporation of a mixed solution of dichloromethane and hexane. Crystallographic data: Δ-*cis*-(N,N)-[Ir(bzq)$_2$(PBO)]; $C_{39}H_{24}IrN_3O_2$, 1.18(CH_2Cl_2), 0.32(C_6H_{14}), FW 886.55, monoclinic, $P2_1$ (#4), a = 9.15927(16) Å, b = 27.4078(5) Å, c = 14.7784(3) Å, α=γ= 90˚, β = 102.475(2)˚, V = 3622.31(12) Å^3, Z = 4, μ = 3.901 mm^{-1}. R_1 = 0.0395 (I > 2σ(I)), wR_2 = 0.0923 (all data), GOF = 1.045 (I > 2σ(I)), Flack parameter = -0.013(3) (CCDC 2063613). Λ-*cis*-(N,N)-[Ir(bzq)$_2$(PBO)]; $C_{39}H_{24}IrN_3O_2$, 1.22(CH_2Cl_2), 0.28(C_6H_{14}), FW 886.58, monoclinic, $P2_1$ (#4), a = 9.15128(17) Å, b = 27.4566(6) Å, c = 14.7617(3) Å, α=γ= 90˚, β = 102.392(2)˚, V = 3622.66(13) Å^3, Z = 4, μ = 3.907 mm^{-1}. R_1 = 0.0434 (I > 2σ(I)), wR_2 = 0.0945 (all data), GOF = 1.039 (I > 2σ(I)), Flack parameter = -0.016(4) (CCDC 2063614).

Single crystals of Λ-*trans*-(N,N)-[Ir(bzq)$_2$(PBO)] was prepared by slow evaporation of a mixed solution of dichloromethane and hexane. Crystallographic data: Λ-*trans*-(N,N)-[Ir(bzq)$_2$(PBO)]; 3($C_{39}H_{24}IrN_3O_2$), 1.5(CH_2Cl_2), FW 2403.82, orthorhombic, $P2_12_12_1$ (#19), a = 10.6678(2) Å, b = 18.2211(4) Å, c = 46.7278(8) Å, α=β=γ= 90˚, V = 9082.9(3) Å^3, Z = 4, μ = 4.541 mm^{-1}. R_1 = 0.0607 (I > 2σ(I)), wR_2 = 0.1098 (all data), GOF = 1.032 (I > 2σ(I)), Flack parameter = -0.018(7) (CCDC 2063616).

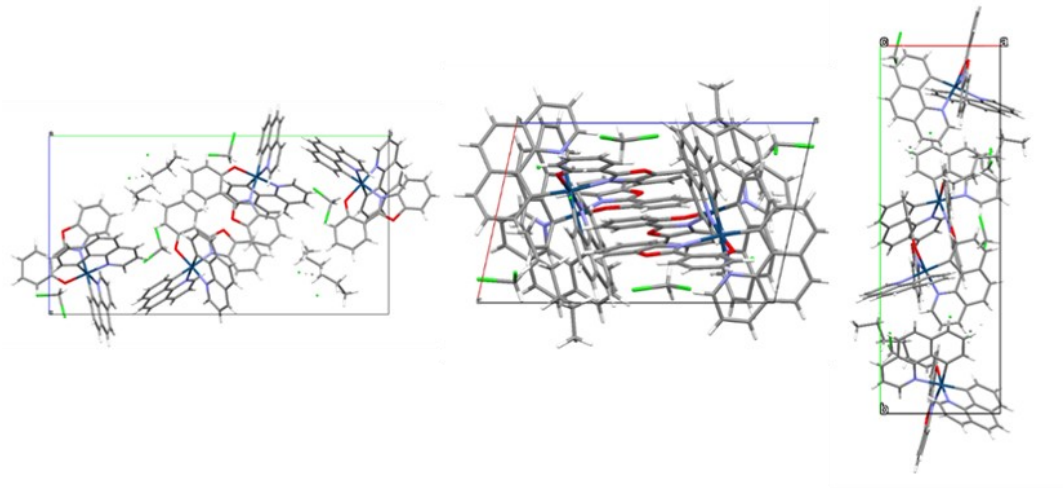

Figure S8. The views of Δ-*cis*-(N,N)-[Ir(bzq)$_2$(PBO)] along the a-axis (left), along the b-axis (middle) and along the c-axis (right), respectively. Solvent molecules are omitted for clarity.

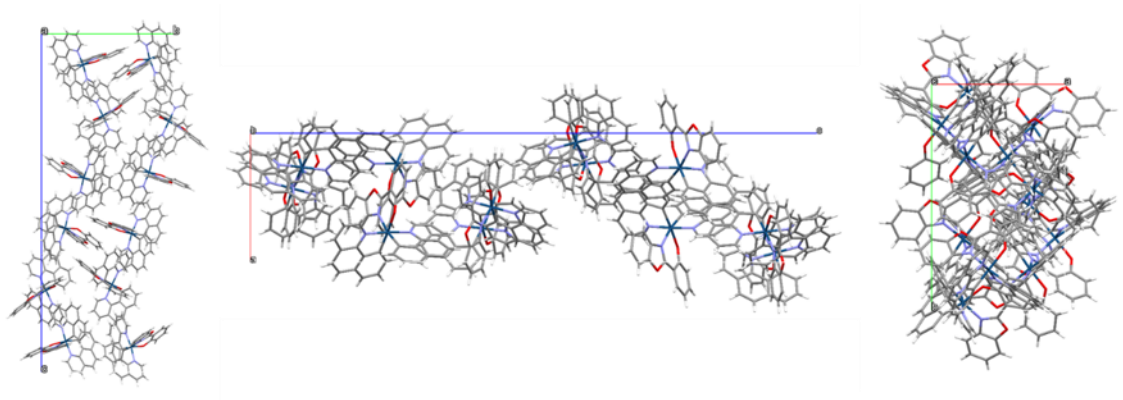

Figure S9. The views of Λ-*trans*-(N,N)-[Ir(bzq)$_2$(PBO)] along the a-axis (left), along the b-axis (middle) and along the c-axis (right), respectively. Solvent molecules are omitted for clarity.

Table S1. Structural information of racemic-*cis*, Δ-, and Λ-*cis*- (N,N) -[Ir(bzq)$_2$(PBO)]

Compound	Racemic-*cis*-(N,N) -[Ir(bzq)$_2$(PBO)]	Δ-*cis*-(N,N)-[Ir(bzq)$_2$(PBO)]	Λ-*cis*-(N,N)-[Ir(bzq)$_2$(PBO)]
Solvent	dichloromethane, hexane	dichloromethane, hexane	dichloromethane, hexane
Formula	$C_{39}H_{24}IrN_3O_2$, CH_2Cl_2	$C_{39}H_{24}IrN_3O_2$, 0.32(C_6H_{14}),1.18(CH_2Cl_2)	$C_{39}H_{24}IrN_3O_2$, 0.28(C_6H_{14}),1.22(CH_2Cl_2)
FW	843.74	886.55	886.58
Crystal system	Triclinic	Monoclinic	Monoclinic
Space group	*P*-1	$P2_1$	$P2_1$
a [Å]	10.4642(3)	9.15927(16)	9.15128(17)
b [Å]	10.5088(2)	27.4078(5)	27.4566(6)
c [Å]	15.5137(4)	14.7784(3)	14.7617(3)
α [deg]	85.981(2)	90	90
β [deg]	76.654(2)	102.475(2)	102.392(2)
γ [deg]	72.389(2)	90	90
V [Å^3]	1582.12(7)	3622.31(12)	3622.66(13)
Z	2	4	4
μ [mm^{-1}]	4.432	3.901	3.907
R_1 ($I > 2\sigma(I)$)	0.0315	0.0395	0.0434
wR_2 (all data)	0.0752	0.0923	0.0945
GOF ($I > 2\sigma(I)$)	1.051	1.045	1.039
Flack parameter	—	-0.013(3)	-0.016(4)
CCDC No.	2063612	2063613	2063614

Table S2. Structural information of racemic-*trans* and Λ-*trans* (N,N) -[Ir(bzq)$_2$(PBO)]

Compound	Racemic-*trans*-(N,N) -[Ir(bzq)$_2$(PBO)]	Λ-*trans*-(N,N)-[Ir(bzq)$_2$(PBO)]
Solvent	dichloromethane, hexane	dichloromethane, hexane
Formula	$C_{39}H_{24}IrN_3O_2$, CH_2Cl_2	3($C_{39}H_{24}IrN_3O_2$), 1.5(CH_2Cl_2)
FW	843.74	2403.82
Crystal system	Triclinic	orthorhombic
Space group	*P*-1	$P2_12_12_1$
a [Å]	12.2740(2)	10.6678(2)
b [Å]	16.9938(3)	18.2211(4)
c [Å]	18.1515(5)	46.7278(8)
α [deg]	106.596(2)	90
β [deg]	109.535(2)	90
γ [deg]	103.187(2)	90
V [Å^3]	3192.42(13)	9082.9(3)
Z	4	4
μ [mm^{-1}]	4.392	4.541
R_1 ($I > 2\sigma(I)$)	0.0426	0.0607
wR_2 (all data)	0.0912	0.1098
GOF ($I > 2\sigma(I)$)	1.022	1.032
Flack parameter	—	-0.018(7)
CCDC No.	2063615	2063616

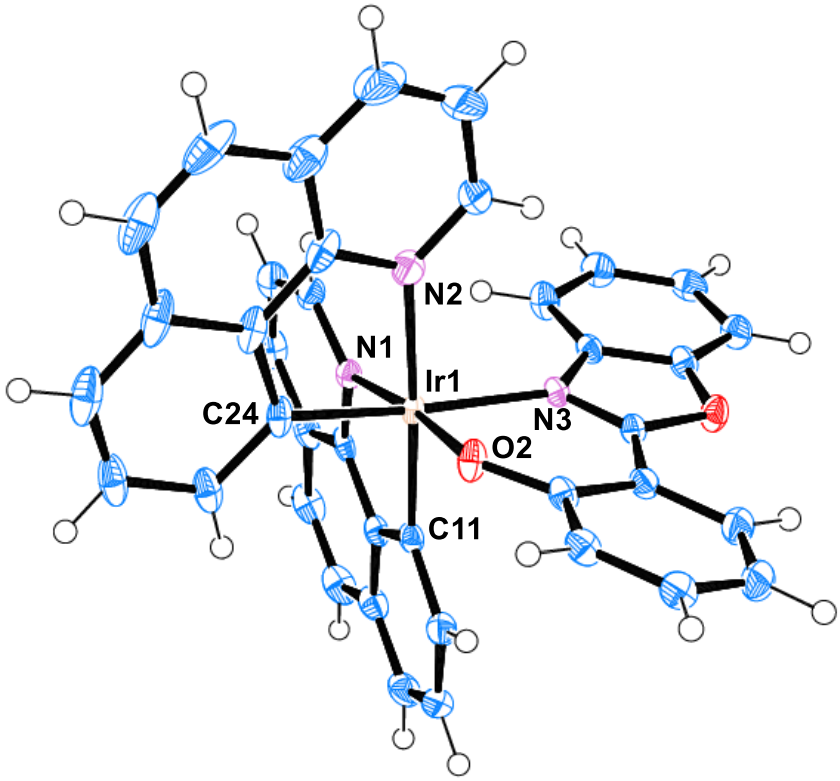

Figure S10. An ORTEP drawing of racemic-*cis*(N,N)-[Ir(bzq)$_2$(PBO)] with a numbering scheme of atoms around a metal ion. The thermal ellipsoids are scaled to the 50% probability level.

Table S3. Selected bond distances (Å) and angles (deg) of racemic-*cis*(N,N)-[Ir(bzq)$_2$(PBO)].

Distance (Å)			
Ir1—O2	2.042 (3)	Ir1—N1	2.025 (3)
Ir1—N2	2.131 (3)	Ir1—N3	2.147 (3)
Ir1—C11	2.007 (4)	Ir1—C24	2.009 (4)

Angle (deg)			
O2—Ir1—N2	86.77 (12)	O2—Ir1—N3	87.54 (11)
N1—Ir1—N2	96.68 (13)	N1—Ir1—N3	97.36 (12)
N2—Ir1—N3	93.47 (12)	C11—Ir1—O2	94.84 (13)
C11—Ir1—N1	81.5 (14)	C11—Ir1—N3	88.97 (13)
C11—Ir1—C24	97.39 (15)	C24—Ir1—O2	88.16 (12)
C24—Ir1—N1	87.36 (13)	C24—Ir1—N2	80.28 (15)

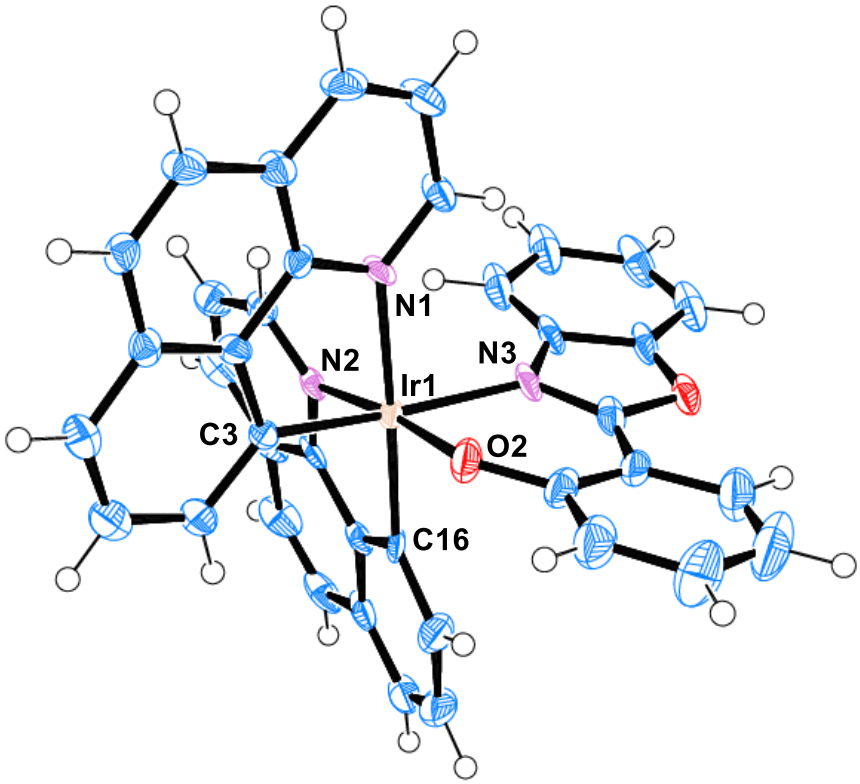

Figure S11. An ORTEP drawing of Δ-*cis*(N,N)-[Ir(bzq)$_2$(PBO)] with a numbering scheme of atoms around a metal ion. The thermal ellipsoids are scaled to the 50% probability level.

Table S4. Selected bond distances (Å) and angles (deg) of Δ-*cis*(N,N)-[Ir(bzq)$_2$(PBO)]

Distance (Å)			
Ir1—O2	2.047 (7)	Ir1—N1	2.132 (7)
Ir1—N2	2.024 (8)	Ir1—N3	2.164 (7)
Ir1—C3	2.011 (8)	Ir1—C16	2.020 (9)

Angle (deg)			
O2—Ir1—N1	87.1 (3)	O2—Ir1—N3	88.3 (3)
N1—Ir1—N3	93.2 (3)	N2—Ir1—N1	96.9 (3)
N2—Ir1—N3	96.4 (3)	C3—Ir1—O2	86.6 (3)
C3—Ir1—N1	80.9 (3)	C3—Ir1—N2	89.1 (3)
C3—Ir1—C16	97.3 (4)	C16—Ir1—O2	94.0 (3)
C16—Ir1—N2	81.9 (3)	C16—Ir1—N3	88.8 (3)

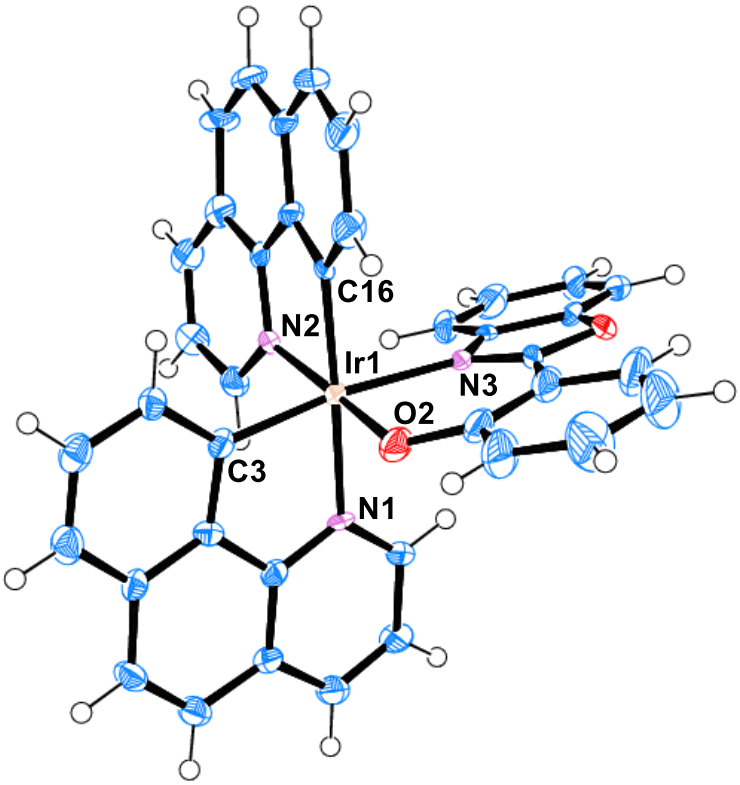

Figure S12. An ORTEP drawing of Λ-*cis*(N,N)-[Ir(bzq)$_2$(PBO)] with a numbering scheme of atoms around a metal ion. The thermal ellipsoids are scaled to the 50% probability level.

Table S5. Selected bond distances (Å) and angles (deg) of Λ-*cis*(N,N)-[Ir(bzq)$_2$(PBO)]

Distance (Å)			
Ir1—O2	2.047 (7)	Ir1—N1	2.132 (7)
Ir1—N2	2.024 (8)	Ir1—N3	2.164 (7)
Ir1—C3	2.011 (8)	Ir1—C16	2.020 (9)

Angle (deg)			
O2—Ir1—N1	87.1 (3)	O2—Ir1—N3	88.3 (3)
N1—Ir1—N3	93.2 (3)	N2—Ir1—N1	96.9 (3)
N2—Ir1—N3	96.4 (3)	C3—Ir1—O2	86.6 (3)
C3—Ir1—N1	80.9 (3)	C3—Ir1—N2	89.1 (3)
C3—Ir1—C16	97.3 (4)	C16—Ir1—O2	94.0 (3)
C16—Ir1—N2	81.9 (3)	C16—Ir1—N3	88.8 (3)

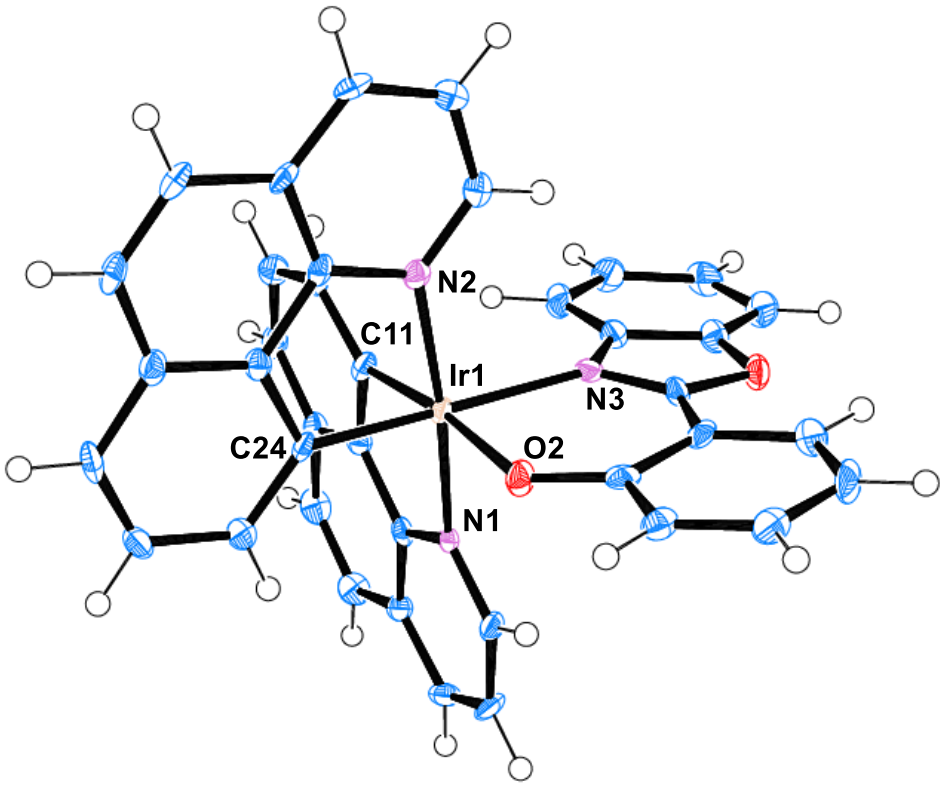

Figure S13. An ORTEP drawing of racemic-*trans*(N,N)-[Ir(bzq)$_2$(PBO)] with a numbering scheme of atoms around a metal ion. The thermal ellipsoids are scaled to the 50% probability level.

Table S6. Selected bond distances (Å) and angles (deg) of racemic-*trans*(N,N)-[Ir(bzq)$_2$(PBO)]

Distance (Å)			
Ir1—O2	2.123 (3)	Ir1—N1	2.035 (4)
Ir1—N2	2.045 (4)	Ir1—N3	2.167 (4)
Ir1—C11	1.994 (5)	Ir1—C24	1.994 (5)

Angle (deg)			
O2—Ir1—N3	87.14 (14)	N1—Ir1—O2	93.20 (15)
N1—Ir1—N3	89.12 (15)	N2—Ir1—O2	90.25 (15)
N2—Ir1—N3	96.07 (15)	C11—Ir1—N1	81.89 (18)
C11—Ir1—N2	94.24 (18)	C11—Ir1—N3	97.34 (18)
C24—Ir1—O2	90.36 (16)	C24—Ir1—N1	93.00 (18)
C24—Ir1—N2	81.95 (18)	C24—Ir1—C11	85.3 (2)

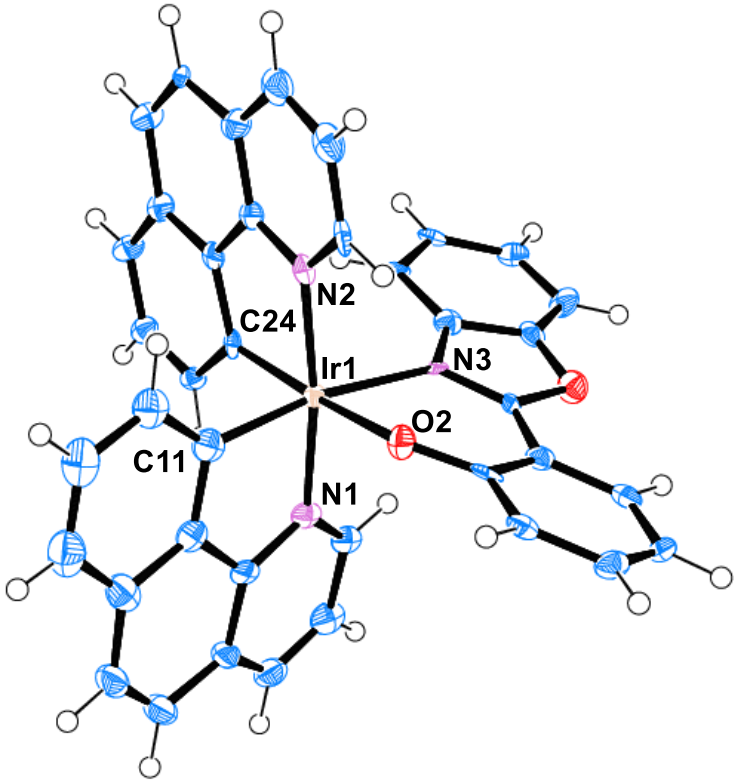

Figure S14. An ORTEP drawing of Λ-*trans*(N,N)-[Ir(bzq)$_2$(PBO)] with a numbering scheme of atoms around a metal ion. The thermal ellipsoids are scaled to the 50% probability level.

Table S7. Selected bond distances (Å) and angles (deg) of Λ-*trans*(N,N)-[Ir(bzq)$_2$(PBO)]

Distance (Å)			
Ir1—O1	2.155 (10)	Ir1—N1	2.031 (12)
Ir1—N2	2.048 (12)	Ir1—N3	2.166 (11)
Ir1—C11	2.008 (17)	Ir1—C24	2.008 (14)

Angle (deg)			
O1—Ir1—N3	84.6 (4)	N1—Ir1—O1	94.8 (4)
N1—Ir1—N3	91.5 (5)	N2—Ir1—O1	91.6 (4)
N2—Ir1—N3	93.9 (4)	C11—Ir1—O1	87.6 (5)
C11—Ir1—N1	81.9 (6)	C11—Ir1—N2	93.7 (5)
C24—Ir1—N1	91.9 (5)	C24—Ir1—N2	81.5 (5)
C24—Ir1—N3	98.5 (5)	C24—Ir1—C11	90.2 (6)

S6. Thermal isomerization of *trans*-(N,N)-[Ir(bzq)$_2$Cl]$_2$

The stereochemically pure *trans*-(N,N)-[Ir(bzq)$_2$Cl]$_2$ which was obtained by a reported procedure was heated in 2-ethoxyethanol/water (1:1) at 110 ˚C for 12 h under a nitrogen atmosphere. A mixture of iridium complexes was quantitatively recovered by precipitation from the reaction mixture and analyzed by using ^{1}H NMR and ESI-MS.

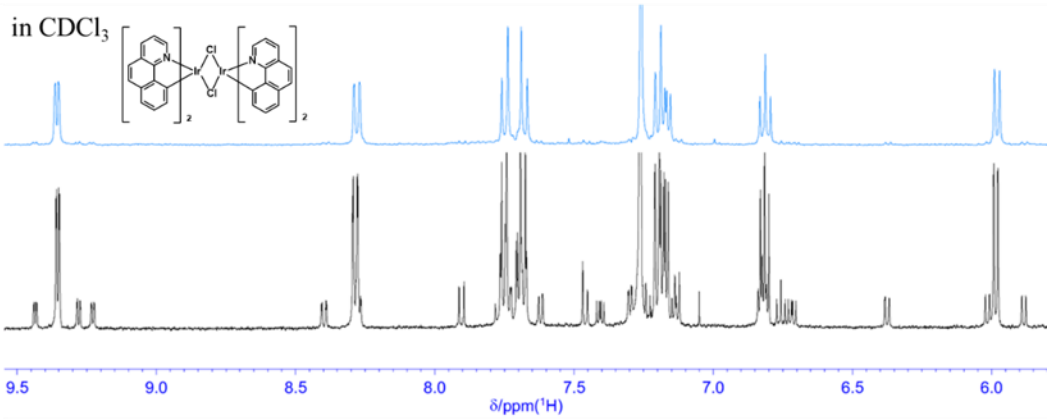

Figure S15. ^{1}H NMR (500 MHz, $CDCl_3$) spectra of synthetic [Ir(bzq)$_2$Cl]$_2$ (top) and a dimeric mixture obtained in 45% of recovery after washing the precipitate with methanol (bottom).

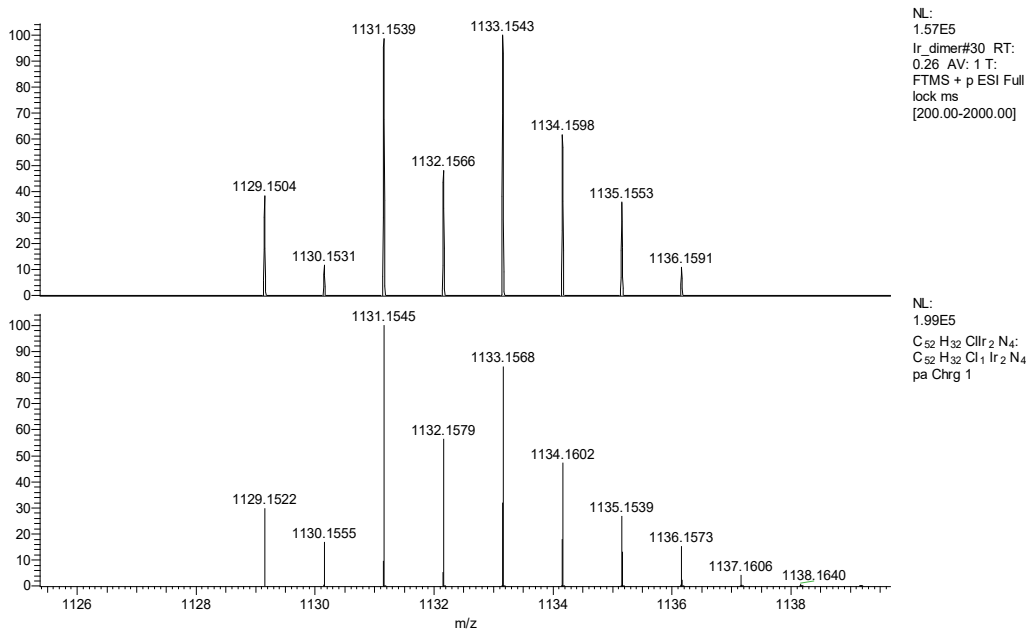

Figure S16. ESI-mass spectra of a crude sample (top) obtained by a thermal experiment and its calculated simulation result (bottom).

S7. Emission properties of [Ir(bzq)$_2$(PBO)]

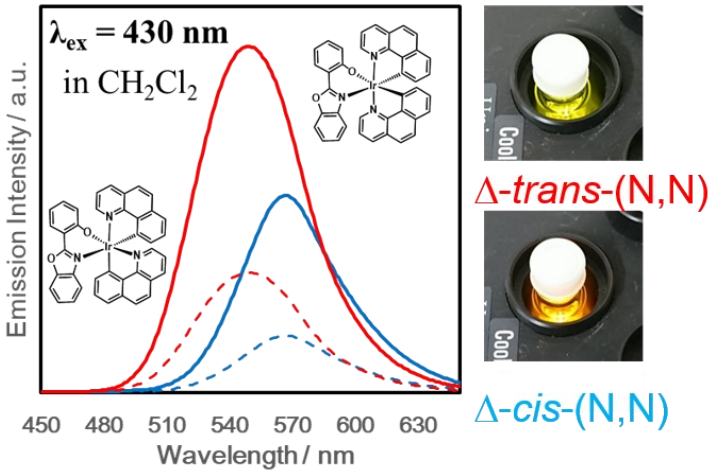

Figure S17. Emission spectra of (blue) *cis*-(N,N) isomer (5.6×10^{-5} M) and (red) *trans*-(N,N) isomer (5.5×10^{-5} M) of [Ir(bzq)$_2$(PBO)] at room temperature. A solvent was CH_2Cl_2. The excitation wavelength was 430 nm. The atmosphere was N_2 (solid line) and air (dotted line). The photo shows the color of emission for each isomer.

S8. Theoretical calculation of energy diagrams of [Ir(bzq)$_2$(PBO)]

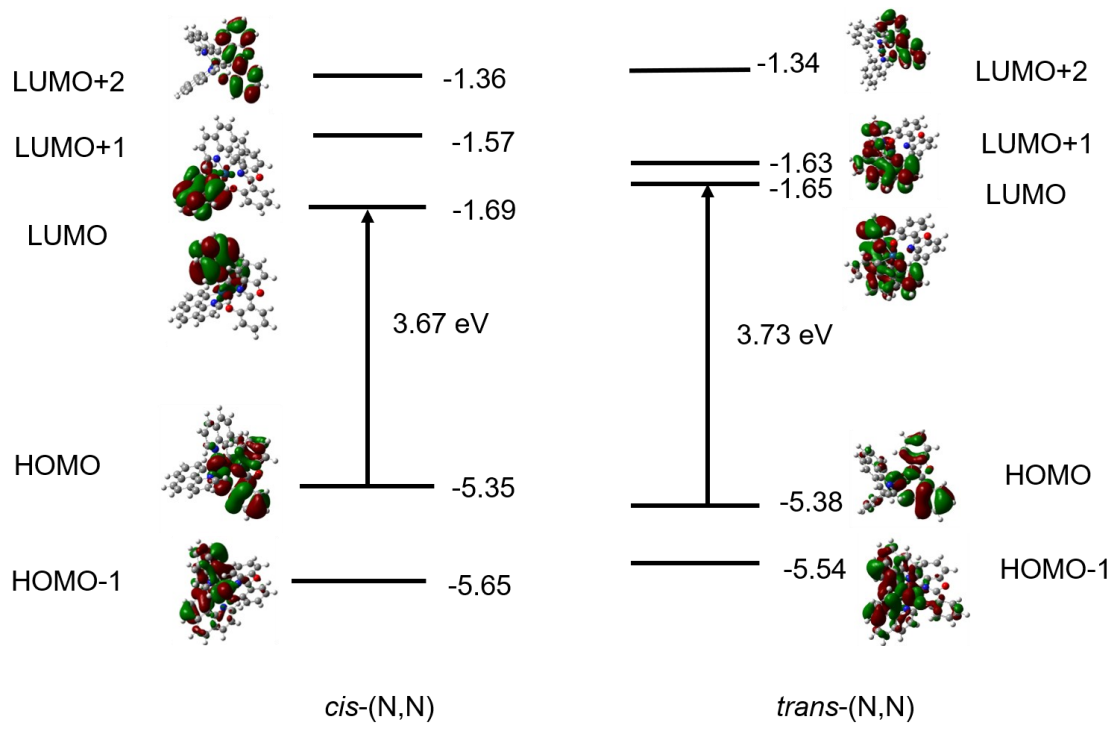

Figure S18. Energy diagrams and molecular orbitals for HOMO-1 to LUMOL+2 based on the DFT ground state calculation: (left) *cis*-(N,N)- and (right) *trans*-(N,N) isomers, respectively.